

POWER COORDINATION CONTROL STRATEGY FOR DISTRIBUTED HYBRID ENERGY STORAGE SYSTEM BASED ON CCS-MPC

ZHIHUA XU¹, ZHANXIANG YIN² AND TINGLONG PAN²

¹School of Electrical Engineering
Yancheng Institute of Technology
No. 1, Hope Avenue Middle Road, Yancheng 224000, P. R. China
xzh@ycit.cn

²School of Internet of Things Engineering
Jiangnan University
No. 1800, Lihu Avenue, Wuxi 214122, P. R. China
6201925029@stu.jiangnan.edu.cn; tlpan@jiangnan.edu.cn

Received April 2023; revised September 2023

ABSTRACT. *Aiming at addressing the problem of coordinated operation in distributed Hybrid Energy Storage Systems (HESS) for DC microgrid systems, a power coordinated control strategy based on Continuous Control Set Model Predictive Control (CCS-MPC) is proposed. The strategy comprises upper and lower layers. The former implements power distribution, using wavelet packet transform to decompose the power demand to the supercapacitors and batteries. Moreover, the adaptive factor is utilized to distribute battery power demand based on the State of Charge (SOC) of the battery to achieve SOC consistency. The lower layer, namely CCS-MPC, uses distributed control, where each DC/DC converter is associated with a model predictive controller. In order to verify the effectiveness of the proposed method, an island DC microgrid model containing distributed HESS was built and compared with the multi-agent consistency control algorithm using a distributed PI controller. The results confirmed that the proposed strategy can effectively reduce DC bus fluctuations and achieve consistent battery SOC faster. In addition, this strategy improves the stability of power grid operation and extends the service life of batteries.*

Keywords: Distributed hybrid energy storage system, Continuous control set, Model predictive control, Power distribution, Wavelet packet transform, SOC consistency

1. Introduction. The effective control of power balance within a DC microgrid is crucial for its stable operation. One important metric for measuring power balance is the stability of DC bus voltage, as indicated by previous studies [1,2]. However, achieving complete power balance between the distributed power supply and the DC load in a DC microgrid is often challenging. Meanwhile, external environment changes and variations in power demand will lead to power fluctuations within the DC microgrid [3,4]. Therefore, energy storage systems are commonly integrated into DC microgrids to buffer power abrupt changes, balance system power and ensure uninterrupted operation of loads [5,6]. Compared with centralized energy storage, distributed energy storage offers advantages such as low cost, high utilization, compatibility and reliability, making it a more flexible option [7,8]. Currently, the energy storage unit is broadly categorized into two types: energy storage and power storage. The former based on batteries, provides long energy storage time and low costs but has a shorter service life. The latter utilizing supercapacitors offers

fast response time and a large number of charge-discharge cycles but comes at a high cost [9,10]. HESS combines with the battery and the supercapacitor technologies. Leveraging their complementary characteristics HESS can smooth instantaneous power fluctuations within the microgrid, reduce the charging and discharging times of the battery to extend its service life and improve the dynamic response of the system [11,12]. Therefore, the research motivations of this paper are mainly focused on two research objectives. Firstly, it aims to tackle the challenge of balancing power within distributed hybrid energy storage systems. Secondly, it seeks to develop an accurate power allocation algorithm for efficiently distributing the given power of each energy storage unit.

Model Predictive Control (MPC) is a control approach commonly employed in converters. It involves analyzing the topological structure model and appropriately handling input/output constraints. The optimal control signal is obtained by solving the value function through an online optimization algorithm [13,14]. In recent years, with the improvement of microprocessor computing power, applications of MPC in power electronic systems have aroused great interest [15,16]. MPC can predict the values of controlled variables, such as voltage, current and stator flux at the next time point through the model. [17] and [18] adopted a current high-performance MPC for permanent magnet synchronous motor drivers. [19] and [20] used Finite Control Set Model Predictive Control (FCS-MPC) to control bus voltage in parallel inverters within a microgrid. [21] proposed a model predictive control method for current control, while not considering bus voltage regulation. [22] proposed a double-layer MPC to solve the problem of extra voltage ripple caused by transient power loss in converters resulting from supercapacitor current in dynamic responses. The upper MPC calculates the optimal power of the lower layer based on the dynamic power loss, while the lower MPC determines the optimal duty ratio of the converter based on the value function and the power loss estimation. [23] proposed an HESS energy management strategy based on Continuous Control Set Model Predictive Control (CCS-MPC), considering the constraints of battery current rate and supercapacitor overvoltage protection, to achieve optimal predictive control of voltage and current. Furthermore, a three-level DC/DC converter control based on MPC is designed in [24]. This converter structure effectively reduces the current ripple and voltage fluctuation during switching device operation. However, MPC under this converter involves eight value functions, which greatly increases the calculation amount.

Compared with existing results, this paper mainly makes the following contributions.

- 1) A coordinated power control strategy based on CCS-MPC is proposed to realize the coordinated control of distributed HESS.
- 2) Wavelet packet transform is used to decompose the power demand, and subsequently, the power allocation for the battery is determined based on the adaptive factor designed for the *SOC* of the battery, ensuring precise distribution of power.
- 3) By designing two schemes, the effectiveness of the control strategy proposed in this paper is verified by comparing and analyzing the dual-loop and CCS-MPC as well as the multi-agent consistency and the battery *SOC* adaptive factor consistency.

The remainder of this paper is organized as follows. Section 2 introduces the distributed HESS structure of DC microgrid. Likewise, Section 3 provides a detailed explanation of the power allocation strategy. Section 4 provides the design and implementation process of the CCS-MPC method. The effectiveness of the algorithm is shown in Section 5. Lastly, the work is concluded in Section 6.

2. Distributed HESS Structure of DC Microgrid. Figure 1 shows the topology of distributed HESS consisting of photovoltaic renewable clean energy, DC load and multiple HESS. The distributed HESS and photovoltaic power generation are connected to the

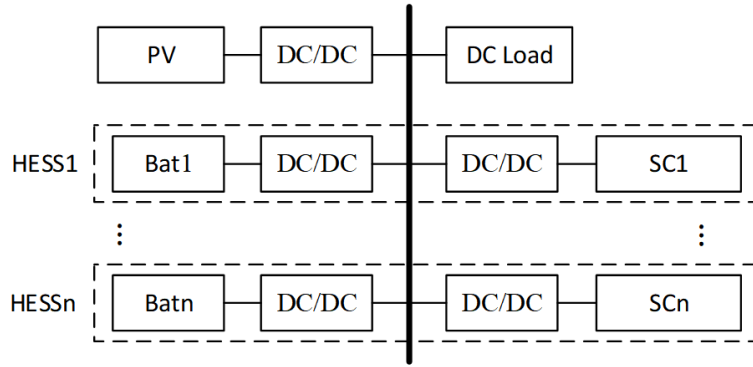


FIGURE 1. Topology of distributed HESS

DC bus through DC/DC converters, while the DC load is directly connected to the DC bus. HESS is used to compensate for the power difference between the distributed power supply and the load, that is, the power demand P_{ref} that HESS needs to meet. According to the characteristics of HESS, P_{ref} must be divided into high and low-frequency components, which are given to the supercapacitor and the battery, respectively. As the battery provides more power than the supercapacitor in the power grid, additional factors, such as the SOC inconsistency of multiple groups of batteries need to be considered in the power distribution of the battery. Considering that the capacity of the battery and the initial SOC are different, the adaptive factor is designed to redistribute the low-frequency part after the wavelet packet transform. This enables batteries with large capacity and high SOC can output more power when discharging or absorb less power when charging, ultimately achieving uniform SOC across multiple batteries. After power distribution, this paper adopts the distributed control of CCS-MPC, where each DC/DC converter corresponds to a model predictive controller. Through the control of voltage and current, the stability of bus voltage and the real-time tracking of power setting might be realized.

3. Power Allocation Strategy.

3.1. Wavelet packet transform. Once the wavelet packet transform decomposes the signal into high-frequency and low-frequency parts, it can not only continue to decompose the low-frequency part, but also decompose the high-frequency part again. Firstly, the wavelet packet decomposition tree is obtained through wavelet packet transform; then the signal is reconstructed with the decomposition tree through the reconstruction of wavelet packet coefficients. A three-layer wavelet packet transform is employed. After performing the decomposition and reconstruction process on P_{ref} , 8 segments of power requirements are obtained as shown in Figure 2, where L is the processed low frequency part, and H is the processed high frequency part.

In the signal values obtained from wavelet packet transformation, it is observed that, except for LLL_3 , the remaining 7 segments exhibit minor fluctuations around zero, indicating that the energy storage unit must undergo frequent charging and discharging to meet the power requirements of these segments, yet excessive energy transfer is not essential. As such, it is most appropriate for the supercapacitor to be responsible. As the simulation verification in this paper uses 5 groups of HESS, the 7 segments are merged as follows:

$$\begin{cases} P_{ref_sc1} = LLH_3 \\ P_{ref_sc2} = LHL_3 \\ P_{ref_sc3} = LHH_3 + HHL_3 \\ P_{ref_sc4} = HLL_3 + HLH_3 \\ P_{ref_sc5} = HHH_3 \end{cases} \quad (1)$$

The LLL_3 is in charge of the battery, and this paper further distinguishes two parameters, namely capacity and initial SOC for the battery part, while the parameters of the super capacitor part are the same. The LLL_3 part will be further allocated below.

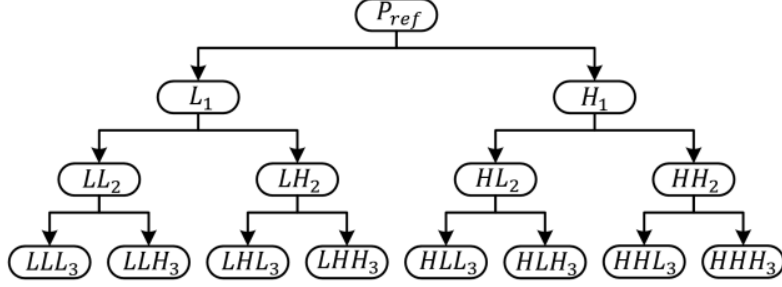


FIGURE 2. Schematic diagram of the three-layer wavelet packet transformation

3.2. Consistent power allocation based on battery SOC adaptive factor. Battery SOC is expressed as [25]

$$SOC = SOC_0 - \frac{\int i_L d\tau}{C_{bt}} = SOC_0 - \frac{\int P_I d\tau}{u_i C_{bt}} \quad (2)$$

where SOC_0 is the initial SOC of the battery. C_{bt} is the capacity of the storage battery. P_I is the output power of the storage battery, which is also the input power of the DC/DC converter. u_i is the output voltage of the battery, which is also the input voltage of the converter. i_L is the inductor current. Among them, the relationship involving P_I is expressed as

$$P_I = u_i i_L = Ri_L^2 + P_o \quad (3)$$

where R is the inductor resistance. P_o is the converter output power. Relative to P_o , R is very small, and its power consumption can be effectively disregarded. As the magnitude of $|P_o|$ increases, the corresponding SOC undergoes a more significant change. Similarly, a larger C_{bt} results in a smaller SOC . When distributing the given power of multiple batteries, the purpose is to achieve uniform SOC levels across multiple batteries. During the discharge phase, a battery with a larger SOC_0 needs to be allocated with a larger power reference at first. When the SOC is consistent, in order to keep the SOC change consistent, the given power distribution is based on C_{bt} .

Assuming the presence of n groups of HESS, the power demand that n storage batteries need to meet is P_{ref_bt} , transformed by wavelet packets for P_{ref} . Firstly, all batteries are sorted from 1 to n according to their SOC_0 . When P_{ref_bt} is positive, all batteries are discharged, and y_i is sequentially set for 1 to $n - 1$ batteries. Conversely, when P_{ref_bt} is negative, all batteries are charged, and y_i is set for n to 2 batteries in reverse order. y_i is related to the SOC and C_{bt} of the battery, and $y_i \in (0, 1)$, denoted as follows:

$$y_i = \begin{cases} a_i - b_i \alpha^{-\rho \Delta SOC_i} & (\Delta SOC_i \geq 0) \\ c_i \alpha^{\rho \Delta SOC_i} + d_i & (\Delta SOC_i < 0) \end{cases} \quad (4)$$

where $\Delta SOC_i = SOC_i - SOC_{i+1}$. α is the difference base number, and $\alpha > 1$. ρ is the difference coefficient. a_i is the maximum value of positive difference consistency. b_i is the consistency coefficient of positive difference. c_i is the consistency coefficient of negative difference. d_i is the consistency maximum value of negative difference. a_i , b_i , c_i and d_i must satisfy the condition $y_i \in (0, 1)$, and the relationship among them is expressed as

$$a_i - b_i = c_i + d_i = \begin{cases} \frac{C_{bti}}{\sum_{\xi=i}^n C_{bt\xi}} & (P_{ref_bt} \geq 0) \\ \frac{C_{bti}}{\sum_{\xi=1}^i C_{bt\xi}} & (P_{ref_bt} < 0) \end{cases} \quad (5)$$

where C_{bti} is the capacity of the i -th storage battery. When $P_{ref_bt} \geq 0$, $i \in \{1, 2, \dots, n-1\}$. When $P_{ref_bt} < 0$, $i \in \{n, n-1, \dots, 2\}$.

In Equation (5), the values of a_i , b_i , c_i and d_i are mainly determined by the capacity of each battery. The values of $a_i - b_i$ and $c_i + d_i$ are the ratio of the capacity of the i -th battery to the sum of the capacities of the batteries when considering the remaining unallocated power. When the battery achieves consistent SOC , the larger its C_{bt} is, the correspondingly larger power can ensure the same SOC change. The reason for calculating the sum of the remaining unallocated battery capacities is that the calculation of y_i is special and will be elaborated below. Each value in a_i , b_i , c_i , and d_i must meet the requirements of the two equations (4) and (5): one is that $y_i \in (0, 1)$ must be satisfied in the distribution, the other is that the sum of the two must be equal to the capacity ratio. When P_{ref_bt} is positive, a_i is first evaluated. Its value cannot be greater than or equal to 1, and its value cannot be smaller. Since a_i represents the upper limit of the adaptive factor y_i , the larger the value, the greater the proportion of power allocation. Therefore, the value of a_i should be as large as possible to make b_i correspondingly large. When P_{ref_bt} is negative, c_i is first evaluated, and its value cannot be less than or equal to 0. Correspondingly, c_i should be made as small as possible to make d_i as large as possible. It can be seen from Equation (5) that when the values of b_i and d_i are as large as possible, as the SOC difference gradually decreases, the change of the adaptive factor y_i also becomes larger accordingly.

According to the positive or negative characteristics of P_{ref_bt} , the power of n storage batteries is determined sequentially by y_i . When P_{ref_bt} is positive, the allocation process starts with battery 1, which has the largest SOC_0 . It is necessary to allocate the maximum power reference, and then directly multiply P_{ref_bt} by y_1 to get the power reference P_{ref_bt1} of battery 1. The remaining allocation, namely $P_{ref_bt} - P_{ref_bt1}$, is multiplied by y_2 to get the power reference P_{ref_bt2} of battery 2. Similarly, the allocation for battery 3 is the remainder after allocating to the first two batteries, namely $P_{ref_bt} - P_{ref_bt1} - P_{ref_bt2}$. By analogy, the factor y_n is not used for the final storage battery n . The remaining allocation after distributing to the first $n-1$ storage batteries represents power reference, P_{ref_btn} , for storage battery n . It can be seen that when P_{ref_bt} is positive, the power of n storage batteries is expressed as

$$\begin{cases} P_{ref_bt1} = P_{ref_bt}y_1 \\ P_{ref_bt2} = P_{ref_bt}(1 - y_1)y_2 \\ \vdots \\ P_{ref_bti} = P_{ref_bt}(1 - y_1)(1 - y_2) \cdots (1 - y_{i-1})y_i \\ \vdots \\ P_{ref_btn-1} = P_{ref_bt}(1 - y_1)(1 - y_2) \cdots (1 - y_{n-2})y_{n-1} \\ P_{ref_btn} = P_{ref_bt}(1 - y_1)(1 - y_2) \cdots (1 - y_{n-2})(1 - y_{n-1}) \end{cases} \quad (6)$$

where P_{ref_bti} is the power reference of the i -th storage battery. When P_{ref_bt} is negative, the power distribution for battery charging is reversed, starting from battery n to battery 1. It can be seen that when P_{ref_bt} is negative, the power of n storage batteries is expressed as

$$\begin{cases} P_{ref_bt1} = P_{ref_bt}(1 - y_n)(1 - y_{n-1}) \cdots (1 - y_3)(1 - y_2) \\ P_{ref_bt2} = P_{ref_bt}(1 - y_n)(1 - y_{n-1}) \cdots (1 - y_3)y_2 \\ \vdots \\ P_{ref_bti} = P_{ref_bt}(1 - y_n)(1 - y_{n-1}) \cdots (1 - y_{i+1})y_i \\ \vdots \\ P_{ref_btn-1} = P_{ref_bt}(1 - y_n)y_{n-1} \\ P_{ref_btn} = P_{ref_bt}y_n \end{cases} \quad (7)$$

To sum up, the block diagram of power distribution control is shown in Figure 3.

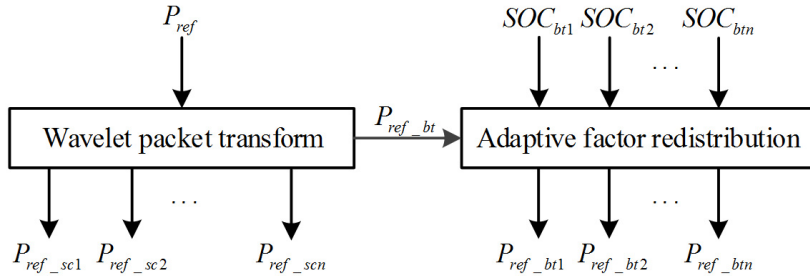


FIGURE 3. Power distribution control block diagram

4. Model Predictive Control.

4.1. Bidirectional DC/DC converter model. The topology of a bidirectional DC/DC converter is depicted in Figure 4. In this paper, we only study two complementary MOS tubes, one in the on state and the other in the state off. When T_1 is on and T_2 is off, the converter operates in Boost mode. The relationship between load voltage u_o and i_L is established as follows:

$$\begin{cases} \frac{di_L}{dt} = \frac{u_i}{L} - \frac{R}{L}i_L \\ \frac{du_o}{dt} = -\frac{1}{CR_L}u_o \end{cases} \quad (8)$$

where L is inductance value, C is load stabilized capacitance and R_L is load resistance. When T_2 is on and T_1 is off, the converter works in Buck mode. The relationship between u_o and i_L is established as follows:

$$\begin{cases} \frac{di_L}{dt} = \frac{u_i}{L} - \frac{R}{L}i_L - \frac{1}{L}u_o \\ \frac{du_o}{dt} = -\frac{1}{CR_L}u_o + \frac{1}{C}i_L \end{cases} \quad (9)$$

The mathematical model of the converter can be obtained by combining (8) and (9), denoted as (10):

$$\begin{cases} \frac{di_L}{dt} = \frac{u_i}{L} - \frac{R}{L}i_L - \frac{1-u}{L}u_o \\ \frac{du_o}{dt} = -\frac{1}{CR_L}u_o + \frac{1-u}{C}i_L \end{cases} \quad (10)$$

where $u = \begin{cases} 1, & S_1 = 1, S_2 = 0 \\ 0, & S_1 = 0, S_2 = 1 \end{cases}$ is the control signal of the model, S_1 is the switch status of T_1 and S_2 is the switch status of T_2 .

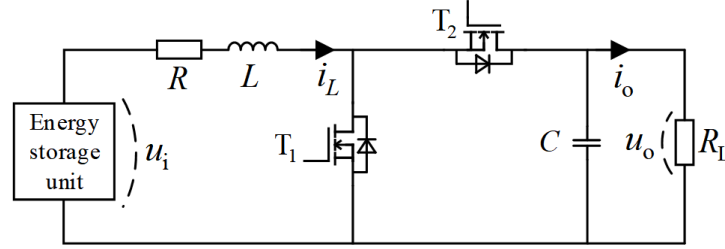


FIGURE 4. Bidirectional DC/DC converter circuit topology

According to the principle of MPC, the sampling period is set as T_S , and the mathematical model of the converter is discretized as Equation (11):

$$\begin{cases} i_L(k+1) = \frac{u_i T_S}{L} + \left(1 - \frac{RT_S}{L}\right) i_L(k) - \frac{[1-u(k)]T_S}{L} u_o(k) \\ u_o(k+1) = \left(1 - \frac{T_S}{CR_L}\right) u_o(k) + \frac{[1-u(k)]T_S}{C} i_L(k) \end{cases} \quad (11)$$

where $u(k) = \begin{cases} 1, & S_1 = 1, S_2 = 0 \\ 0, & S_1 = 0, S_2 = 1 \end{cases}$ is the model control signal after discretization. As MPC is considered a lower-level control, it is desirable to have a smaller value of T_S in order to achieve a faster control response.

By denoting $x(k) = [i_L(k) \quad u_o(k)]^T$, $y(k) = x(k)$, the discrete model (11) can be represented as a matrix form, as shown in Equation (12) [23]:

$$\begin{cases} x(k+1) = Ax(k) + Bu(k) + C \\ y(k) = Dx(k) \end{cases} \quad (12)$$

$$\text{where } A = \begin{bmatrix} 1 - \frac{RT_S}{L} & -\frac{T_S}{L} \\ \frac{T_S}{C} & 1 - \frac{T_S}{CR_L} \end{bmatrix}, B = \begin{bmatrix} \frac{T_S}{L} u_o(k) \\ -\frac{T_S}{C} i_L(k) \end{bmatrix}, C = \begin{bmatrix} \frac{u_i T_S}{L} \\ 0 \end{bmatrix}, D = I.$$

4.2. CCS-MPC strategy. Given the bidirectional DC/DC model, as illustrated in Equation (12), the goal of control is to drive $x(k)$ towards a predetermined reference value. To achieve this, the reference values of u_o and i_L are initially determined as $r(k) = [i_{Lref}(k) \quad u_{ref}(k)]^T$.

Since distributed HESS is connected to the DC bus in parallel via the converter, the reference value u_{ref} of u_o is the given value of the bus voltage. By analyzing Formula (3), it is found that it is a quadratic equation of a single variable about i_L . As a result, i_{L0} can be solved as

$$i_{L0} = \frac{u_i - \sqrt{u_i^2 - 4RP_{ref}}}{2R} \quad (13)$$

To meet the requirements of both voltage control and power control, additional compensation terms for voltage error and power error are incorporated based on i_{L0} . This is done in order to improve the dynamic performance of the control system and reduce the steady-state error when the load changes abruptly. The compensation items of voltage

error ε_u and power error ε_P are as follows:

$$\begin{cases} \varepsilon_u = K_{Pu}\Delta u + K_{Iu} \int \Delta u d\tau \\ \varepsilon_P = K_{PP}\Delta P + K_{IP} \int \Delta P d\tau \end{cases} \quad (14)$$

where $\Delta u = u_{ref} - u_o$, $\Delta P = P_{ref} - P_o$, K_{Pu} , K_{PP} are proportional coefficients of compensating voltage error and power error, respectively. K_{Iu} , K_{IP} are the compensation integral coefficients of voltage error and power error. Thus, the reference value i_{Lref} of i_L is expressed as follows:

$$i_{Lref} = i_{L0} + \varepsilon_u + \varepsilon_P \quad (15)$$

Then the reference vector $r(k) = [i_{Lref}(k) \quad u_{ref}(k)]^T$ for $x(k)$ is determined according to the given value. The error between the reference value and the actual value is denoted as

$$e(k) = r(k) - x(k) \quad (16)$$

To predict the K step in MPC, u_o and i_L at time $k+1$ can be calculated using Formula (12). Subsequently, by substituting the calculated value at time $k+1$ into Formula (12), u_o and i_L at time $k+2$ can be determined. This process continues until u_o and i_L at time $k+k$ can be calculated. Ultimately, the prediction of $x(k)$ is expressed as follows:

$$\begin{cases} x(k+1) = Ax(k) + Bu(k) + C \\ x(k+2) = A^2x(k) + ABu(k) + Bu(k+1) + (A+1)C \\ \vdots \\ x(k+i) = A^ix(k) + A^{i-1}Bu(k) + A^{i-2}Bu(k+1) + \dots + Bu(k+i-1) \\ \quad + (A^{i-1} + A^{i-2} + \dots + 1)C \\ \vdots \\ x(k+K) = A^Kx(k) + A^{K-1}Bu(k) + A^{K-2}Bu(k+1) + \dots + Bu(k+K-1) \\ \quad + (A^{K-1} + A^{K-2} + \dots + 1)C \end{cases} \quad (17)$$

A suitable number of predicted steps K should be carefully chosen. A small value of K facilitates rapid realization of predictive control with swift responsiveness. However, a disadvantage is the diminished anti-jamming ability due to the limited number of predictive steps. Conversely, a larger value of K enhances the control capability and anti-interference of the system, but the dynamic response speed is reduced due to the increase of the number of predicted steps. The above equation needs to be transformed into a state-space equation:

$$\begin{cases} X(k) = Fx(k) + GU(k) + H \\ Y(k) = X(k) \end{cases} \quad (18)$$

$$\text{where } X(k) = \begin{bmatrix} x(k+1) \\ x(k+2) \\ \vdots \\ x(k+K) \end{bmatrix}, F = \begin{bmatrix} A \\ A^2 \\ \vdots \\ A^K \end{bmatrix}, G = \begin{bmatrix} B & & & \\ AB & B & & \\ \vdots & & \ddots & \\ A^{K-1}B & A^{K-2}B & \dots & B \end{bmatrix}, U(k) = \begin{bmatrix} u(k) \\ u(k+1) \\ \vdots \\ u(k+K-1) \end{bmatrix}, H = \begin{bmatrix} C \\ (A+1)C \\ \vdots \\ \sum_{j=0}^{K-1} A^j C \end{bmatrix}.$$

The steady-state error is measured by the variance between the reference value and the actual value. Moreover, the control of the actual value is closely related to the control

signal, leading to their integration into the value function of MPC, as expressed in (19):

$$\left\{ \begin{array}{l} J = J_1 + J_2 \\ J_1 = q \sum_{i=1}^K \{ [i_L(k+i) - i_{Lref}(k)]^2 + [u_o(k+i) - u_{ref}(k)]^2 \} \\ J_2 = w \sum_{j=0}^{K-1} [u(k+j)]^2 \end{array} \right. \quad (19)$$

where q , w are weight coefficients, respectively. In the above equation, $i_L(k+i)$ and $u_o(k+i)$ are the predicted value from time $k+1$ to time $k+K$. The variance sum between the predicted value and the reference value at time k is one of the important components of the value function of model predictive control. Additionally, the sum of the squares of the control signal $u(k+i-1)$ at time k and time $k+K-1$ is added into the value function to reflect the fluctuation degree of the predicted value. By assessing the importance of the two elements in achieving the control objective, the values of the two elements are determined, with the larger value indicating the primary control target. In this paper, in order to achieve coordinated power distribution while maintaining a stable bus voltage, q is much larger than w .

Convert the above value function into a matrix form:

$$J = E(k)^T Q E(k) + U(k)^T W U(k) \quad (20)$$

where $E(k) = R(k) - X(k)$. $R(k) = \begin{bmatrix} r(k) \\ r(k) \\ \vdots \\ r(k) \end{bmatrix}$, $Q = \begin{bmatrix} q & & & \\ & q & & \\ & & \dots & \\ & & & q \end{bmatrix}$, $W = \begin{bmatrix} w & & & \\ & w & & \\ & & \dots & \\ & & & w \end{bmatrix}$.

In simulation, $q = 10$, $w = 0.1$.

One obtains (21) through calculation:

$$\begin{aligned} J &= [R(k) - Fx(k) - GU(k) - H]^T Q [R(k) - Fx(k) - GU(k) - H] + U(k)^T W U(k) \\ &= [R(k) - Fx(k) - H]^T Q [R(k) - Fx(k) - H] - 2 [R(k) - Fx(k) - H]^T Q G U(k) \\ &\quad + U(k)^T (G^T Q G + W) U(k) \end{aligned} \quad (21)$$

where $U(k)$ is the variable. Obviously, the above equation is a quadratic function of $U(k)$. Since J is the sum of three squares, in order to minimize J , the derivative of J with respect to $U(k)$ is set to be zero, i.e., $\partial J / \partial U(k) = 0$. Finally, the value of $U(k)$ can be obtained as

$$U(k) = (G^T Q G + W)^{-1} G^T Q [R(k) - Fx(k) - H] \quad (22)$$

Take the first data of $U(k)$ as the control signal inputting to the converter, i.e., $U(1)$. $U(1)$ is treated as the duty ratio of PWM after the limiting process. Subsequently, the control signal of DC/DC converter is achieved. The block diagram of the bottom CCS-MPC is shown in Figure 5. The bottom layer adopts CCS-MPC. The power of P_{ref_sci} and P_{ref_bt} is given as input, and the control signals of MOS tube in DC/DC converter are directly obtained from the output of CCS-MPC, namely $f_{sci.1}$ and $f_{sci.2}$ and $f_{bti.1}$ and $f_{bti.2}$.

5. Simulation Verification and Result Analysis. The photovoltaic DC micro grid model with energy storage system is built and verified by simulations. The following two schemes have been utilized for comparative analysis.

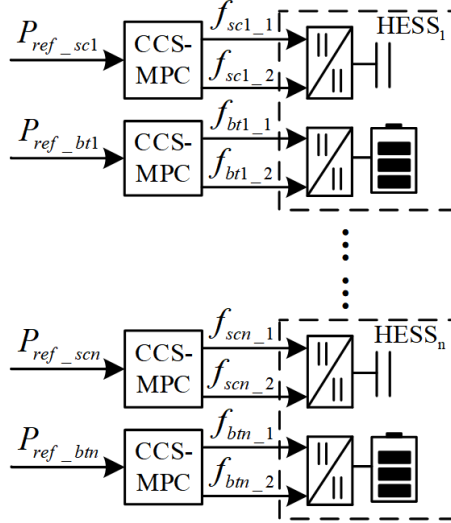


FIGURE 5. Distributed HESS control block diagram

1) Scheme 1: The control object is the photovoltaic DC microgrid with distributed HESS, and the control strategy is power distribution control based on the consistency of multi-agent.

2) Scheme 2: The control object is the photovoltaic DC microgrid with distributed HESS, and the control strategy is the one proposed in this paper.

The control objectives of the two schemes center around isolated DC micro-grid featuring five sets of HESS. In the upper control, both schemes decompose the power demand P_{ref} through wavelet packet transform to obtain the power settings of five supercapacitors. For the battery part, Scheme 1 adopts the multi-agent consensus strategy, while Scheme 2 adopts the control strategy in Section 3.2 of this paper. In the lower control layer, Scheme 1 adopts a double closed-loop control for voltage and current, whereas Scheme 2 adopts CCS-MPC strategy. The level of wavelet packet transform operates at level 3. The primary control objective for both schemes is to meet the power demand of the system while ensuring consistency in the SOC across batteries with different capacity and initial SOC levels, all while maintaining stability in DC bus voltage. A comparative assessment based on bus voltage, energy storage unit output power, and battery SOC values confirms the significance of HESS and validates the efficacy of the proposed HESS control scheme in this study. The parameters of the control object model under two schemes are consistent. The main simulation model parameters are shown in Table 1. The power demand P_{ref} that the energy storage systems in both schemes are required to meet is shown in Figure 6. This paper mainly studies the control of the energy storage system, while the photovoltaic power generation and DC load are not the focus of this paper. In the simulation of the two schemes, the PV power generation has a stable output power of 100 kW. The simulation results of the two schemes are shown in Figures 7-10.

Figure 7 shows the DC bus voltage curve. It can be seen that the bus voltages of both schemes are above or below 500 V, realizing the bus voltage stability of the microgrid. In contrast, the voltage jitter of the double closed-loop is large, especially during the charging of the energy storage system. Scheme 2 displays minimal voltage jitter and fewer waveform burrs, indicating its superiority over Scheme 1.

Figure 8 shows the output power curve of five batteries in the energy storage system. The supercapacitor assists in mitigating the power demand fluctuations experienced by the batteries by absorbing the high-frequency component of the power demand. After

TABLE 1. The main simulation parameters of DC microgrid

Parameter symbol	Parameter value	Parameter description
U_{ref}	500 V	DC bus reference voltage
$SOC_{1(0)}$	80%	Initial SOC of battery 1
$SOC_{2(0)}$	79%	Initial SOC of battery 2
$SOC_{3(0)}$	78%	Initial SOC of battery 3
$SOC_{4(0)}$	77%	Initial SOC of battery 4
$SOC_{5(0)}$	76%	Initial SOC of battery 5
C_{bt1}	16 Ah	Capacity of battery 1
C_{bt2}	24 Ah	Capacity of battery 2
C_{bt3}	16 Ah	Capacity of battery 3
C_{bt4}	16 Ah	Capacity of battery 4
C_{bt5}	12 Ah	Capacity of battery 5
L	5 mH	Inductance value
R	0.02 Ω	Inductance resistance
C	0.01 F	Load voltage stabilizing capacitor
$SOC_{sc(0)}$	80%	Initial SOC of supercapacitor
C_{sc}	8 F	Rated capacitance of supercapacitor

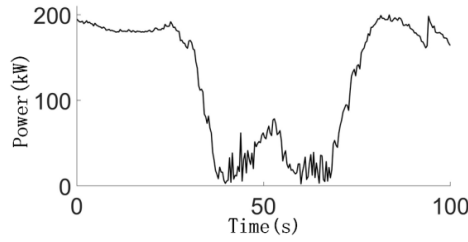


FIGURE 6. Power demand curve that the energy storage system needs to meet

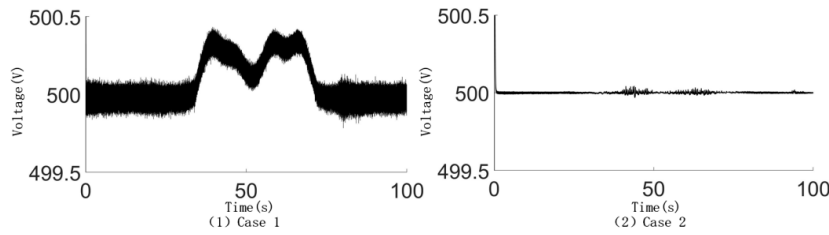


FIGURE 7. DC link voltage curve

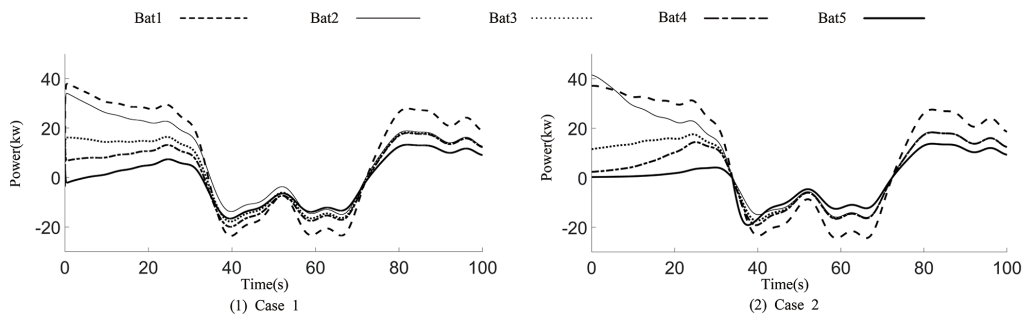


FIGURE 8. Battery output power curve

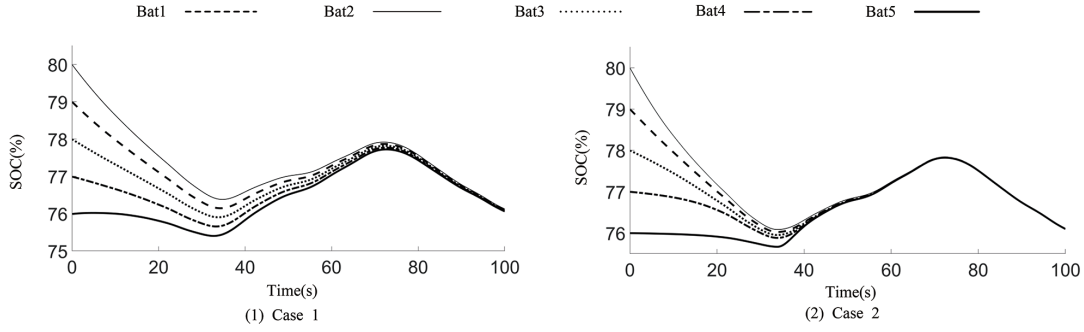
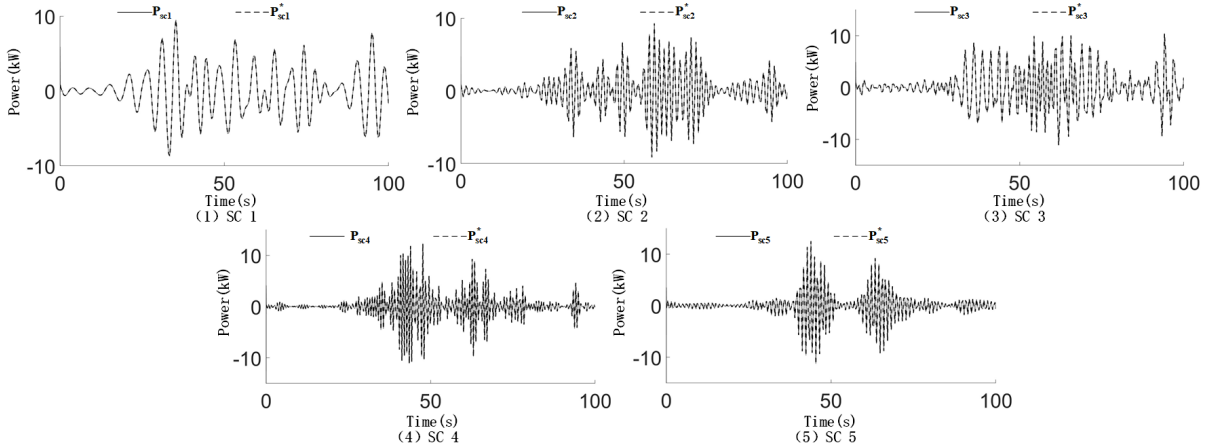
FIGURE 9. Battery *SOC* curve

FIGURE 10. Given power curve and output power curve of the supercapacitor in Scheme 3

power distribution, each battery bears a smaller fluctuation in power, ensuring the stable operation of the microgrid system. It can be seen from Figure 8(1) that the output power curve is relatively rough due to the large fluctuations of the bus voltage in Scheme 1.

Figure 9 shows the *SOC* curves of three batteries. It can be seen from the analysis of Equation (2) and Equation (3) that the greater absolute value $|P_o|$ of battery output power, the greater changes of *SOC*. By referring to Figure 8, we can analyze Figure 9. The *SOC* value of battery 1 is the largest, and the capacity value of battery 2 C_{bt} is the largest. It can be seen in Figure 8 that the output power of battery 1 of Scheme 1 is the largest at the initial time, and the output power of battery 2 of Scheme 2 is the largest. Once the *SOC* of the last five batteries in Figure 9(2) becomes consistent, battery 2, with its larger capacity (C_{bt}), needs to output more power than the other batteries. Conversely, battery 5 must output the least power compared to the other batteries. Additionally, since the capacities of batteries 1, 3, and 4 are the same, the output power of the last three batteries is also identical. It can be seen from the comparison of the two schemes in Figure 9 that the power allocation method in this paper is better than that of the multi-agent consensus approach. Under the same power demand, Scheme 2 achieves *SOC* consistency around 60 s, while Scheme 1 is close to achieving consistency until the end of simulation. The two schemes take the *SOC* difference between batteries as the main reference for power distribution. From the P_{bt5} waveform in Figure 8(1), it can be seen that the control parameters of Scheme 1 have been the optimal values. Combined with Figure 8(1) and Figure 9(1), when the *SOC* difference is small, the reduction of *SOC* difference between batteries is slow, resulting in similar output power of batteries 1, 3 and 4. Compared

with Figure 8(2) and Figure 9(2), when the *SOC* difference is not 0, the output power of battery 5 in Scheme 2 is less than that in Scheme 1, and other batteries bear more power output. Therefore, the *SOC* difference between batteries in Scheme 2 undergoes more noticeable changes. It can be seen that the *SOC* difference between batteries in the power distribution strategy plays a greater role than that in Scheme 1. Although multi-agent consensus can ultimately achieve battery *SOC* consistency, the strategy designed proposed in this paper is better.

Figure 10 shows the output power curve of the five supercapacitors. The thicker black dotted line is the reference power, and the thinner black solid line is the output power of the supercapacitor. Since both schemes assign the same power to each supercapacitor, the five supercapacitors in the two schemes follow the power assignment well and meet the high-frequency part of the power demand. Consequently, only one group of supercapacitors' output power and power assignment diagram is displayed.

6. Conclusion. In this paper, we investigate an isolated-island DC microgrid featuring distributed HESS and propose a power coordinated control strategy based on CCS-MPC for the energy storage system. The strategy involves two layers, with CCS-MPC at the lower layer and a power allocation strategy at the upper layer. Upon determining the power demand required to compensate for the distributed HESS, the power demand of the energy storage system is decomposed using wavelet packet transform to compensate for the supercapacitor and battery. Considering the battery capacity and the initial *SOC* are different, we design a power distribution method based on battery *SOC* adaptive factors, leading to the redistribution of the battery to achieve *SOC* consistency. Following the allocation of designed power of each energy storage unit, CCS-MPC optimizes the output stable voltage of the energy storage unit and real-time power setting values through online prediction. Two simulation schemes are designed in this paper, and the two-layer control methods are compared with other control methods: CCS-MPC and a voltage and current double closed-loop, battery *SOC* based adaptive factor consistent power distribution method and multi-agent consistent control. The simulation results indicate that when the energy storage system encounters the complex power demand, CCS-MPC yields certain voltage fluctuations but small voltage jitter. Furthermore, the power distribution method based on battery *SOC* adaptive factor consistency proposed in this paper can achieve faster battery *SOC* consistency. In conclusion, the power coordination control strategy based on CCS-MPC proposed in this paper proves to be effective for isolated-island DC microgrids with distributed HESS.

Although many scholars are currently working on simplified model predictive control methods in an attempt to reduce the computational burden of model prediction, when the prediction step size is large, it will still affect the real-time performance of the algorithm. The subsequent research focus of this article will give priority to combining the event-triggering mechanism with the model predictive control method to improve real-time performance.

REFERENCES

- [1] Q. Xu, J. Xiao, X. Hu, P. Wang and M. Y. Lee, A decentralized power management strategy for hybrid energy storage system with autonomous bus voltage restoration and state-of-charge recovery, *IEEE Transactions on Industrial Electronics*, vol.64, no.9, pp.7098-7108, 2017.
- [2] C. Zhou, Y. Shen and Z. Wang, Research on vibration suppression of transmission chain in wind power generation system with gear clearance based on internal model control, *International Journal of Innovative Computing, Information and Control*, vol.18, no.4, pp.1247-1263, 2022.

- [3] J. Dixon, I. Nakashima, E. F. Arcos and M. Ortúzar, Electric vehicle using a combination of ultracapacitors and ZEBRA battery, *IEEE Transactions on Industrial Electronics*, vol.57, no.3, pp.943-949, 2010.
- [4] S. Zhang, R. Xiong and F. Sun, Model predictive control for power management in a plug-in hybrid electric vehicle with a hybrid energy storage system, *Applied Energy*, vol.185, pp.1654-1662, 2017.
- [5] Y. Sun, Z. Zhao, M. Yang, D. Jia, W. Pei and B. Xu, Overview of energy storage in renewable energy power fluctuation mitigation, *CSEE Journal of Power and Energy Systems*, vol.6, no.1, pp.160-173, 2020.
- [6] B.-H. Nguyen, R. German, J. P. F. Trovão and A. Bouscayrol, Real-time energy management of battery/supercapacitor electric vehicles based on an adaptation of Pontryagin's minimum principle, *IEEE Transactions on Vehicular Technology*, vol.68, no.1, pp.203-212, 2019.
- [7] X.-K. Liu, H. Jiang, Y.-W. Wang and H. He, A distributed iterative learning framework for DC microgrids: Current sharing and voltage regulation, *IEEE Transactions on Emerging Topics in Computational Intelligence*, vol.4, no.2, pp.119-129, 2020.
- [8] M. Masih-Tehrani and M. Dahmardeh, A novel power distribution system employing state of available power estimation for a hybrid energy storage system, *IEEE Transactions on Industrial Electronics*, vol.65, no.8, pp.6676-6685, 2018.
- [9] Q. W. Xu, X. L. Hu, P. Wang, J. F. Xiao, P. F. Tu, C. Y. Wen and M. Y. Lee, A decentralized dynamic power-sharing strategy for hybrid energy storage system in autonomous DC microgrid, *IEEE Transactions on Industrial Electronics*, vol.64, no.7, pp.5930-5941, 2017.
- [10] A. Dehghanzadeh, G. Farahani, H. Vahedi and K. Al-Haddad, Model predictive control design for DC-DC converters applied to a photovoltaic system, *International Journal of Electrical Power & Energy Systems*, vol.103, pp.537-544, 2018.
- [11] U. Manandhar, N. R. Tummuru, S. K. Kollimalla, A. Ukil, G. H. Beng and K. Chaudhari, Validation of faster joint control strategy for battery and supercapacitor-based energy storage system, *IEEE Transactions on Industrial Electronics*, vol.65, no.4, pp.3286-3295, 2018.
- [12] Y. H. Shan, J. F. Hu, K. W. Chan, Q. Fu and J. M. Guerrero, Model predictive control of bidirectional DC-DC converters and AC/DC interlinking converters – A new control method for PV-wind-battery microgrids, *IEEE Transactions on Sustainable Energy*, vol.10, no.4, pp.1823-1833, 2019.
- [13] N. Korada and M. K. Mishra, Grid adaptive power management strategy for an integrated microgrid with hybrid energy storage, *IEEE Transactions on Industrial Electronics*, vol.64, no.4, pp.2884-2892, 2017.
- [14] N. Guler, S. Biricik, S. Bayhan and H. Komurcugil, Model predictive control of DC-DC SEPIC converters with auto-tuning weighting factor, *IEEE Transactions on Industrial Electronics*, vol.68, no.10, pp.9433-9443, 2021.
- [15] P. Karamanakos, E. Liegmann, T. Geyer and R. Kennel, Model predictive control of power electronic systems: Methods, results, and challenges, *IEEE Open Journal of Industry Applications*, vol.1, pp.95-114, 2020.
- [16] J. Hu, Y. Shan, J. M. Guerrero, A. Ioinovici, K. W. Chan and J. Rodriguez, Model predictive control of microgrids – An overview, *Renewable and Sustainable Energy Reviews*, vol.136, DOI: 10.1016/j.rser.2020.110422, 2021.
- [17] X. Sun, M. Wu, G. Lei, Y. Guo and J. Zhu, An improved model predictive current control for PMSM drives based on current track circle, *IEEE Transactions on Industrial Electronics*, vol.68, no.5, pp.3782-3793, 2021.
- [18] X. Zhang, L. Zhang and Y. Zhang, Model predictive current control for PMSM drives with parameter robustness improvement, *IEEE Transactions on Power Electronics*, vol.34, no.2, pp.1645-1657, 2019.
- [19] C. H. Young and A. Bastias, Finite-control-set predictive voltage control of paralleled inverters in an islanded microgrid, *2018 IEEE 27th International Symposium on Industrial Electronics (ISIE)*, pp.395-400, 2018.
- [20] V. Yaramasu, M. Rivera, M. Narimani, B. Wu and J. Rodriguez, Model predictive approach for a simple and effective load voltage control of four-leg inverter with an output LC filter, *IEEE Transactions on Industrial Electronics*, vol.61, no.10, pp.5259-5270, 2014.
- [21] X. N. Zhang, B. F. Wang, U. Manandhar, H. B. Gooi and G. Foo, A model predictive current-controlled bidirectional three-level DC/DC converter for hybrid energy storage system in DC microgrids, *IEEE Transactions on Power Electronics*, vol.34, no.5, pp.4025-4030, 2019.
- [22] X. B. Zhang, B. F. Wang, D. Gamage and A. Ukil, Model predictive control based dynamic power loss prediction for hybrid energy storage system in DC microgrids, *IEEE Transactions on Industrial Electronics*, vol.69, no.8, pp.8080-8090, 2022.

- [23] N. D. Nguyen, C. Yoon and Y. I. Lee, A standalone energy management system of battery/supercapacitor hybrid energy storage system for electric vehicles using model predictive control, *IEEE Transactions on Industrial Electronics*, vol.70, no.5, pp.5104-5114, 2023.
- [24] Y. Mei, X. Q. Li and Y. Y. Qi, A model predictive control method for three-level bi-directional DC-DC converter in renewable generation system, *2015 18th International Conference on Electrical Machines and Systems (ICEMS)*, Pattaya, pp.417-421, 2015.
- [25] Y. J. Hong, D. Z. Xu, W. L. Yang, B. Jiang and X. G. Yan, A novel multi-agent model-free control for state-of-charge balancing between distributed battery energy storage systems, *IEEE Transactions on Emerging Topics in Computational Intelligence*, vol.5, no.4, pp.679-688, 2021.

Author Biography



Zhihua Xu received the B.Eng. degree in Electronic Information Engineering from Jiangnan University, Wuxi, China, in 2003, and the M.Eng. degree in Control Theory and Control Engineering with Jiangnan University, Wuxi, China, in 2011.

He is currently a Lecturer with Yancheng Institute of Technology. His research interests include new energy generation technology, energy storage technology, electronic technology design and application and signal analysis and processing.



Zhanxiang Yin received the B.S. degree in Automation from Nanjing Institute of Technology, Nanjing, China, in 2019, and the M.Eng. degree in Electrical Engineering with Jiangnan University, Wuxi, China, in 2023.

He is currently a software engineer in Shanghai, working in the photovoltaic inverter industry. His research interests include microgrid control technology, energy storage technology and smart grid.



Tinglong Pan received his B.Eng. degree in Industrial Automation from China University of Mining and Technology, Xuzhou, China, in 1999, and the Ph.D. degree in Power Electronics and Power Drive from China University of Mining and Technology, Xuzhou, China, in 2004.

He is currently a Professor at Jiangnan University. His research interests include microgrid control technology, power conversion technology, power drive system and its intelligent control technology.